

THE EFFECTS OF DELAYED ETTRINGITE FORMATION ON THE EXPANSION OF A MASSIVE BRIDGE PIER AND A PRECAST PRESTRESSED CONCRETE BEAM OF A BRIDGE

Bruno Godart^{1*}, Othman Omikrine-Metalssi¹, Badreddine Kchakech¹,
Stephane Lavaud¹

¹Université Paris Est - IFSTTAR, Marne La Vallée, France

Abstract

This article shows that Delayed Ettringite Formation (DEF) may affect massive parts of concrete structures as well as precast structural members through the presentation of two examples: a massive pier column and a precast prestressed concrete beam. For each of them the article presents a brief description of the structure, detailed information on the distress mechanism and cracking involved, residual expansion results obtained on concrete cores extracted, the assessment through the use of FEM analysis, considering a new model implemented in CESAR-LCPC software, and the recommended actions for their management including monitoring.

The results highlight that the exposure conditions and the temperature reached provided a significant effect on the displacements and stresses of the structures affected by DEF.

Keywords: delayed ettringite formation, expansion, cracking, assessment, FEM analysis.

1 INTRODUCTION

Internal swelling reactions (ISR) caused by Delayed Ettringite Formation (DEF) can severely damage concrete structures. Primary ettringite (a hydrous calcium trisulphoaluminate) is a normal reaction product formed from the reaction of C3A and C4AF with gypsum within the early ages of the concrete while the hydration of Portland cement. However, when the concrete temperature reaches important values of about 65°C, the sulphates may be incorporated in other cement phases. Indeed, the rise in temperature modifies the condition of sulphate equilibrium between the sulphate hydrates and the hydrated calcium silicates (C-S-H). When the temperature of a concrete rises during setting, sulphates are trapped by physical adsorption on C-S-H. The adsorption capacity of sulphate ions is high and is directly related to the basicity of the pore solution of the concrete and to the temperature of the heat treatment: a higher pH and temperature favour adsorption. This latter is reversible, and if the conditions inside concrete are modified during time, the sulphates are released and lead to the formation of secondary (delayed) ettringite [1]. After concrete hardening, the very slow formation of secondary ettringite may occur as water is incorporated into the crystal structure which can lead to potentially deleterious expansion. DEF is defined as the formation of ettringite in the concrete after setting, and without any external sulphate supply, but water. This mechanism normally appears in concrete exposed to high humidity conditions (or directly in contact with water), subjected to a relatively high thermal treatment (i.e. temperatures > 65°C) or having reached similar temperatures for whatever other reasons than thermal curing (e.g. massive cast-in-place concrete, concrete casting during summer, etc).

The expansive process leads to macroscopic local effects similar to those created by Alkali-Aggregate Reaction (AAR) and mainly consisting in material swelling, cracking and decreasing of the mechanical properties which may cause large structural disorders due to unexpected deformations and additional stresses in concrete and reinforcement [2,3].

The prediction of concrete expansion and deterioration, and the assessment of the efficiency of remedial solutions are crucial points for existing affected structures whose serviceability and structural safety may constitute serious concerns [4]. In this context, in order to provide useful guidelines for structure owners, tools for accurately assessing the real condition of affected structures as well as its evolution over time are needed. Furthermore, the French Institute of Science and Technology for Transport, Development and Networks (Ifsttar, formerly LCPC) has developed the RGIB (Réaction de Gonflement Interne du Béton: Internal swelling reaction of concrete) module in

* Correspondence to: bruno.godart@ifsttar.fr

the CESAR-LCPC Finite Element-code allowing the reassessment of DEF affected structures, taking into account several thermo-hydro-chemo-mechanical couplings [5,7] such as: influence of thermo-hydric conditions, effects of the early age thermal history, anisotropy of the imposed expansion related to the direction of concrete casting, damage resulting from cracking of the material, drying shrinkage, creep and coupling between the expansion and the state of stresses.

This paper describes the investigations conducted in two structures through the use of Ifsttar FEM for elucidating management decisions of DEF affected structures.

2 CASE OF A MASSIVE BRIDGE PIER

2.1 Description of the structure

The massive pier P1, part of a viaduct that supports a motorway, was built in 2003. This viaduct is composed by a continuous structure having 4 spans with respectively lengths of 30.80 m, 50.05 m, 50.05 m and 30.80 m, as well as width of 13 m. The deck, constituted by a concrete slab connected onto two steel girders, is resting on three piers (P1, P2 and P3) and two abutments (Figure 1). Each pier is of the "T" shape and is composed of a cap beam placed on top a cylindrical shaft having a diameter of 3 m and a height of 4.10 m. The cap beam is 12.80 m long and has a variable thickness and height. All the pier footings are immersed into the river, whereas only piers P1 and P2 are partially immersed. It should be noticed that the cap-beams of the 3 piers have been strengthened by post-tensioning a short time after the construction of the viaduct because of an error in the structure design (Figure 2). This work is focused on pier P1 which is actually the structural member most affected by DEF. The diagnosis of DEF was established after a careful examination of concrete cores taken out of the piers with the help of Scanning electron microscopy (SEM).

2.2 Damage observed and instrumentation of the pier

The pier P1 presents several vertical cracks and a regular crazing on its full height (Figure 3). A detailed inspection was conducted by CONCRETE Company in 2012 and some cracks were instrumented by studs and their openings followed with the help of an extensometer. This system allows to record regularly (at each observation) the crack openings with a precision of 1/100 mm. In March 2005, sixteen pairs of studs were installed in some cracks of the piers, whose width were in between 0.1 and 0.3 mm ; eight years later, the average width increased reached 0.15 mm, and the maximal increase was 0.3 mm. This instrumentation showed clearly that pier P1 expansion is active.

Reference frames made up of four axes plotted in a zone of one square meter were also installed on the pier facings in order to measure and follow the cracking index according to LCPC method n°47 [8]. Temperature recording was also performed simultaneously to the crack opening measures. The reference frames on P1 have been installed in August 2010. From 2010 to 2013, the cracking index measurement increased from 0.17 to 0.44 mm/m, which remains in the range of low values. The maximum crack's opening was 0.2 mm. (Figure 3).

Strain gauges have been installed recently in order to monitor the strains in the reinforcement bars. Three gauges were fixed on each of the three hoops AR2 to AR4, and six other gauges were fixed on the vertical bars (Figure 4).

2.3 Methods for assessment and analysis

In order to help the structure owners in their management decisions, it is necessary to design tools aimed to accurately appraise the real damaged degree of aging structures as well as its potential future distress. In this context, the RGIB module of CESAR-LCPC was used. Taking advantage of the geometric and boundary conditions symmetry, only a quarter of the structure was modelled. A total of 16889 three dimensional elements and 24279 nodes were used for the entire finite element model.

The concrete properties Young's modulus, Poisson's ratio and density were respectively assumed to be: $E_c = 35000$ MPa, $\nu = 0.20$, and $\rho = 2400$ kg / m³. Compressive and tensile strengths at 28 days were assumed to be 35 MPa and 2.7 MPa, respectively. The numerical analysis was conducted over a period of 25 years. The main geometric characteristics and the finite element mesh used for the simulations are shown in Figure 5.

Thermal simulation

A simulation using the TEXO module of CESAR-LCPC software was used to evaluate the thermal history at the construction period (TEXO allows the calculation of a temperature field developing in a concrete member during setting). The concrete thermal properties were obtained through adiabatic tests on reconstituted concrete samples. The thermal conductivity was selected

constant and equal to $K=1.66 \text{ W/m} \cdot ^\circ\text{C}$, the thermal capacity of this concrete was adopted equal to $2400 \text{ Wh/m}^3 \cdot ^\circ\text{C}$ and the coefficient of thermal exchange was $\lambda=6 \text{ W/m}^2 \cdot ^\circ\text{C}$ because of the use of metal formwork.

Figure 6 shows that the temperature reached about $83 \text{ }^\circ\text{C}$ in the middle of the pier and stayed higher than $70 \text{ }^\circ\text{C}$ during a little more than 5 days, while the temperature reached a value of $53 \text{ }^\circ\text{C}$ at the pier surface. These results are clearly consistent with the development of DEF in the pier column.

Humidity simulation

Beyond that, the finite-element code CESAR-LCPC was used to calculate the evolution of the relative humidity inside the structural member. The ambient relative humidity was supposed to be 85% in the cap beam and the upper part of the pier, whereas it was considered equal to 100 % in the lower part of the pier and footings since they are always immersed in water. The initial internal humidity of the concrete was adopted of being 95%.

Figure 7 shows the evolution of the saturation degree vs. time for some points located in the pier at the tidal zone. The values ranged from 0.88 and 0.98 at this part of the structure which might provide an effect on the expansion of the pier. The periodic variations on some curves are due to the consideration of the seasonal variation of the water level of the river.

Residual expansion of concrete

In order to feed the swelling parameters of the calculation model, the estimation of the future possible expansion is needed. This latter is derived from a residual expansion test of concrete cores in accordance with the testing method previously developed by LCPC [9]. Thus, one core was taken in the middle of each pier P1 and P2, in the area where the pier is subjected to the highest temperature. The test results, presented in Figure 8, demonstrate that the maximal residual expansion in pier P1 reaches about 0.6%.

Principles of the computational reassessment

Over the framework of the methodology elaborated for the expertise of Internal Swelling Reaction (ISR) -affected concrete structures [10-11], a method of computational reassessment was developed. It consists in calibrating the parameters of the chemical induced expansion kinetics, from the information collected on the damaged structure (cracking index and global deformation) and from possible additional tests on reconstituted or existing concrete [12].

Following the theoretical developments proposed by Li [12], the total deformation is the summation of the elastic deformation, the plastic deformation, the deformation due to shrinkage and creep, and the chemical induced deformation. The chemically-induced part of the deformation for DEF is derived from Larive's law [13] successively improved by Brunetaud and is based on equation 1. In this equation, ε_∞ corresponds to the final expansion, τ_c and τ_l are the characteristic and the latency times respectively (corresponding to the swelling rate and the duration before the onset of expansion), φ and δ are two complementary parameters introduced by Brunetaud into the Larive's law [14] to model an asymptotically linear phase at the end of the reaction which is more relevant for DEF. In the case of pier P1, the values of the expansion parameters were then determined:

$\tau_c = 93 \text{ days}$, $\tau_l = 183 \text{ days}$ and $\varepsilon_\infty = 1\%$.

$$\varepsilon(t) = \varepsilon_\infty \cdot \frac{1 - e^{-\frac{t}{\tau_c}}}{1 - e^{-\frac{(t-\tau_l)}{\tau_c}}} \cdot \left\{ \begin{array}{ll} 1 & \text{for AAR} \\ 1 - \frac{\varphi}{\delta + t} \text{ with } 0 \leq \varphi \leq \delta & \text{for DEF} \end{array} \right\} \quad (1)$$

This model can then be implemented in a FEM software such as CESAR-LCPC (RGIB module). The chemo-mechanical computation is based on the results of two complementary modeling: one aimed at assessing the temperature field in the structure, and the other one consisting in solving the transient non-linear moisture-diffusion equation governing the evolution of humidity in the porous network of the structure.

Results of the reassessment

Considering the effect of anisotropy and stiffness reduction, Figure 9 displays the current iso-values of displacements in the transversal and vertical directions. The vertical displacement at the top of the cap beam reaches a maximum value of about 10 mm, while the transversal displacements reach 9 mm. The transversal swelling is more significant in the lower part of the pier where the saturation degree is higher (immersion of the pier in the river). This result highlights the relationship between

expansion and water content in the concrete structure. These results show also that even the parts of the cylindrical pier (the lower and upper extreme zones) that have not been overheated at early age are affected by swelling imposed by the expansion of the centre of the pier. The extremities of the pier are also restrained by the absence of internal expansion of the footing and the cap beam.

Concerning the values and the evolution of stresses in the steel reinforcement, which is one of the most important indicators of the mechanical behaviour of the pier, the results show that, after a latency period, the swelling of the structure causes tensions in the steel bars which become quite important in the case of vertical (AR_6) and circular (AR_3, AR_4 and AR_5) bars, where the swelling is greater. The values of the tensile stresses in these reinforcing steel bars exceed 800 MPa for the final expansion, whereas they don't exceed 330 MPa in AR_1 and 500 MPa in AR_2 (Figure 10). In these calculations, a purely elastic behavior of steel bars has been assumed; however, in reality, such stresses cannot develop in the reinforcement and then the results have to be interpreted as an incursion of steel in the field of plasticity. Finally, the results confirm that the tensile stresses in the reinforcing steel bars will probably exceed the yielding threshold after about three years.

In order to check whether this calculation is reliable and conservative, strain gauges have been recently installed on the rebars. The first results (Figure 11) confirm that some rebars are subjected to significant elongations; it is the case for gauges J6 and J7 glued on the circular bar AR_3 which indicates a stress increase of about 50 MPa within sixteen months.

3 CASE OF A PRECAST PRESTRESSED CONCRETE BEAM OF A BRIDGE

3.1 Description of the structure

The bridge was built in 1995 and is composed of a continuous structure having four spans with lengths of 9.700 m, 14.275 m, 11.275 m and 9.700 m respectively and a width of 13 m. The deck, resting on two abutments and three piers, is composed of 4 x 11 precast beams (9 internal beams and 2 edge beams) connected to a general reinforced concrete slab which is continuous on piers. A cross-section of the studied bridge is given in Figure 12.

3.2 Damage observed and instrumentation of the bridge

The detection of deterioration (cracks and expansion) occurred some years after construction only on those edge beams particularly exposed to high humidity (rain). The rest of the structure seems not affected by this swelling. The cracking on the external face of the edge beams is mainly longitudinal (Figure 13) and relatively important, particularly at the ends, but the highest crack width (0.5 mm) is observed in the centre of the beams. Cracking on the internal face of the edge beams is much less important, and all nine internal beams are free of cracks. The diagnosis based on SEM analysis was made by IFSTTAR and confirmed that the edge beam is only affected by DEF (no AAR gels are present and the aggregates are non reactive).

In January 2011, two methods for the monitoring of expansion and cracking [15] have been used on the edge beams of the bridge. The first one is the measure of global deformations by using studs on the depth of three sections of an edge beam and on the whole length of the beam. The second one is the installation of several reference frames on the external face of some edge beams in order to measure and follow up the cracking index according to LCPC method n°47 [8].

3.3 Methods for assessment and analysis

The modelling calculations were conducted with the RGIB module of CESAR LCPC and were focused only on a quarter of the structure due to the symmetry of the geometric and boundary conditions. The numerical simulations have been performed, assuming concrete Young's modulus and Poisson's ratio equal to $E_c = 40500$ MPa and $\nu = 0.20$ respectively. Density of concrete was adopted as $\rho = 2400$ kg / m³. Compressive and tensile strengths at 28 days are assumed to be 50 and 4.4 MPa, respectively. The duration of the analysis is 30 years. A total of 200,204 volume elements and 293,223 nodes were used in the entire model for finite elements calculations. The main geometrical characteristics and the finite element mesh used for the simulations are shown in Figure 14.

The bridge was subjected to different loadings: dead and live loads (i.e. own weight and traffic loading and longitudinal prestressing forces introduced in the 11 precast beams). As for the boundary conditions, the transverse displacements were restrained on both symmetry faces of the model. Finally, the reinforcing steel bars in these beams were considered with a Young modulus of 210 GPa.

Thermal simulation

The thermal simulation was a difficulty of the assessment because there was only partial information from the precast plant in the bridge file. Particularly, the heating cycle applied to the

concrete during its setting was not known and it was decided to consider in this assessment three heat treatments with an imposed temperature T_{imp} respectively equal to 50 °C, 60 °C and 65 °C. As in the previous case, the simulation was conducted with the same values of concrete thermal properties. Indeed, the early age temperature of the concrete in the beam increased with the raise of the heat treatment, and the results show that it reached a maximum value of respectively 79 °C, 82 °C and 83.5 °C for an imposed temperature of the heat treatment T_{imp} respectively equal to 50°C, 60°C and 65 °C. These maximum values of the temperature are clearly consistent with the formation of DEF.

Humidity simulation

The finite-element code CESAR-LCPC was also used to calculate the humidity evolution. For that purpose, the ambient relative humidity was supposed to be 85% in the 9 internal beams and the internal faces of the edge beams, while it is considered equal to 95 % in the rest of the structure. The initial internal relative humidity of the concrete was taken equal to 90% and the duration of the analysis is 30 years as in the case of mechanical calculations.

Residual expansion of concrete

The results of the residual expansion test conducted on 7 cores extracted from the edge beams showed that there is some heterogeneity between the different cores drilled from one beam to another and a significant development of ettringite with a maximum residual expansion value of 0.43% was found. The swelling parameters of the model were calibrated from the residual expansion curve giving the free expansion of the core taken from the studied pier and the evolution of the cracking index determined from in-situ measurements. The values of the expansion parameters were then determined. For this study, the following values were used: $\tau_c = 111$ days; $\tau_L = 342$ days; $\varepsilon_\infty = 1.3\%$.

Results of the reassessment

Figure 16 displays the iso-values of the vertical displacements of the deck at the present time (2014) for the three suggested temperatures. The deflections of the edge beams are much more important than those of the inner beams. A comparison of the results for the three heat treatments shows an obvious increase of displacements with higher temperature conditions. This result confirms that the thermal conditions of precast have a direct influence on the deck expansion and therefore a more realistic modelling would require very accurate data on the precast conditions.

Moreover, a comparison of vertical displacements between the inner and outer faces of the edge beams (Figure 15) shows that the vertical displacements of the external surface (surface exposed to a high humidity) are somehow leveling off, while those in the inner surface are increasing and will probably reach the same values as the external surface after a decade. This finding may suggest a gradual development of new cracks in the inner parts of the edge beams.

An analysis of the evolution of stresses in the steel reinforcement highlights that, after a latency period, the concrete expansion causes tensions in the steel bars (Figure 17). The tensions in the vertical steel bars increase from the end of the edge beam (where its value reaches 200 MPa at AR1) to the mid span of the bridge where its value exceeds 900 MPa at AR 5). However, these tensile values don't exceed 100 MPa in the longitudinal steel bars (AR 6). In these simulations, we assume a purely elastic behavior of steel bars, but in reality, such stresses cannot develop in the reinforcement that is subjected to plasticity.

4 CONCLUSIONS

Both case studies highlight the effect of DEF on the overall and local behaviour of the structures. Massive parts and precast products are most vulnerable to this reaction, depending on the temperature reached in the concrete during the setting. The determination of the mechanical condition of the structure depends necessarily on the variation of stresses in the different reinforcing steel bars, and in both cases, the results confirm that the tensile stresses in some reinforcing steel bars will exceed the yielding threshold. Therefore, the decision of strengthening the structures may become necessary in order to increase their life-time, but it should be taken after confirmation of the predicted evolution by a thorough monitoring of the evolution of cracking, global deformations and steel strains.

5 REFERENCES

- [1] Divet, L, Randriambololana, R (1998): Delayed Ettringite Formation: the effect of temperature and basicity on the interaction of sulphate and C-S-H phase. *Cement and Concrete Research*, 28(3), 357-363.

- [2] Omikrine Metalssi, O, Godart, B, and Toutlemonde, F (2013): Effectiveness of Nondestructive Methods for the Evaluation of Structures Affected by Internal Swelling Reactions: A Review of Electric, Seismic and Acoustic Methods Based on Laboratory and Site Experiences. *Experimental Techniques*, DOI: 10.1111/ext.12010.
- [3] Omikrine –Metalssi, O, Seignol, JF, Rigobert, S, and Toutlemonde F (2014): Modelling the crack opening-closing and possible remedial sawing operation of AAR-effected dams. *Engineering Failure Analysis*, **36**, 199-214.
- [4] Leroy, R, Boldea, LI, Seignol, JF, and Godart, B (2011): Re-assessment of an ASR affected gravity dam. In: *Dams and Reservoirs under changing Challenges*, Lucerne, Switzerland.
- [5] Sellier, A, Bourdarot, E, Multon, S, Cyr, M, and Grimal, E (2009): Combination of structural monitoring and laboratory testing for assessment of alkali-aggregate reaction swelling: application to gate structure dam. *ACI Materials Journal*, **106** (3) 281-290.
- [6] Baghdadi, N, Toutlemonde, F, and Seignol, JF (2008): Chemo-mechanical model describing the expansion due to internal sulphate attack: numerical simulation. In: *Concrete modelling CONMOD'08*, Delft, (The Netherlands), May 26-28, RILEM PRO 58, 291-298.
- [7] Seignol, JF, Baghdadi, N, and Toutlemonde, F (2009): A macroscopic chemo-mechanical model aimed at re-assessment of DEF affected concrete structures. 1st Int. Conf. on computational technologies in concrete structures, Jeju, Korea, 422-440.
- [8] LCPC (1997): Détermination de l'indice de fissuration d'un parement de béton. Techniques et méthodes, Méthode d'essai LPC No. 47. Ministère de l'Équipement, du Logement, des Transports et du Tourisme.
- [9] Pavoine, A, Divet, L, (2009): Réaction sulfatique interne au béton : Essai d'expansion résiduelle sur carotte de béton extraite de l'ouvrage. Méthode d'essai n° 67, Techniques et méthodes des laboratoires des ponts et chaussées, Méthode d'essai ME67 - 28p.
- [10] LCPC (2003): Aide à la gestion des ouvrages atteints de réaction de gonflement interne. Guide technique, Paris, 2003.
- [11] Multon, S, Barin, FX, Godart, B, Toutlemonde, F (2008): Estimation of the residual expansion of concrete affected by alkali silica reaction. *Journal of Materials in Civil Engineering*, **20** (1), pp 54-62.
- [12] Li, K, and Coussy O (2002): Concrete ASR degradation: from material modelling to structure assessment. *Concrete Science and Engineering*, **4**, pp 34-46.
- [13] Larive, C, (1999): Apports combinés de l'expérimentation et de la modélisation à la compréhension de l'alkali-réaction et de ses effets mécaniques. ERLPC OA28, LCPC, Paris.
- [14] Brunetaud, X (2005): Etude de l'influence de différents paramètres et de leurs interactions sur la cinétique et l'amplitude de la réaction sulfatique interne au béton. Thèse de l'Ecole Centrale Paris.
- [15] LCPC (2009): Méthodes de suivi dimensionnel et de suivi de la fissuration des structures - Avec application aux structures atteintes de réaction de gonflement interne du béton", Guide technique.

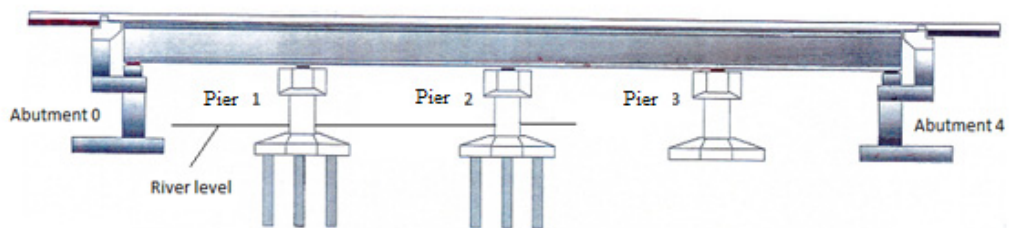


FIGURE 1: General view of the viaduct.



FIGURE 2: View of the Pier P1 with the cap beam strengthened by prestressing tendons.

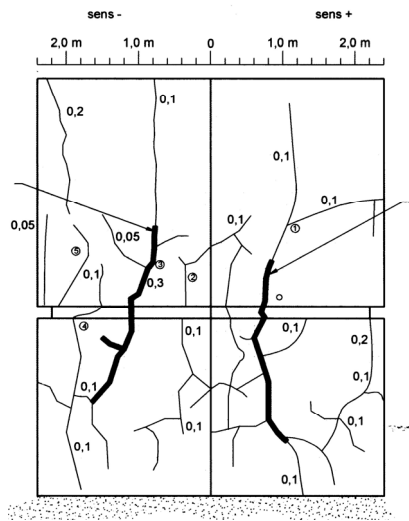


FIGURE 3: Cracking at the surface of the pier P1 (the thick lines correspond to injected cracks – crack width in mm).

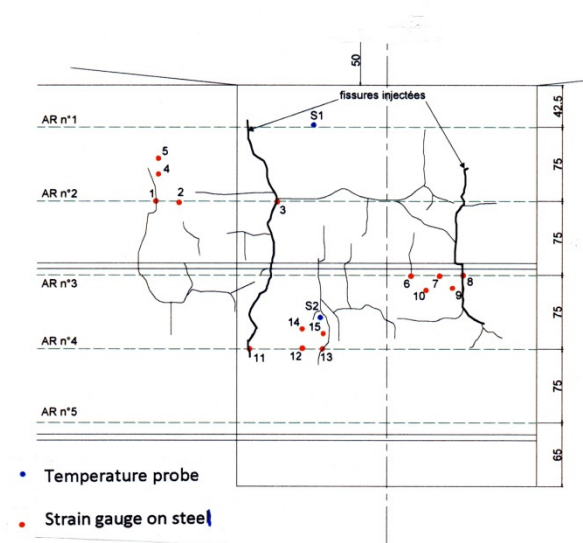


FIGURE 4: Location of strain gauges J1 to J15 (on hoops and vertical bars) and temperature probes S1 and S2.

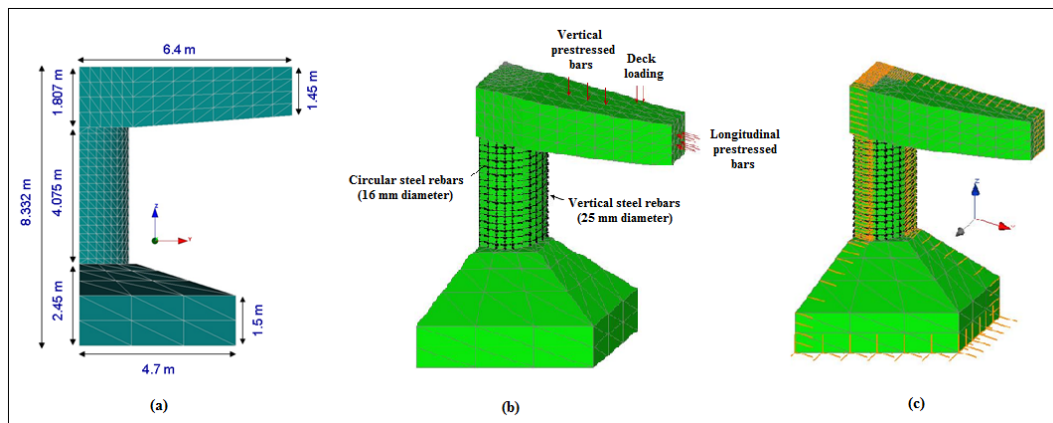


FIGURE 5: Presentation of the pier dimensions (a), applied loadings on cap beam (b) and boundary conditions (c).

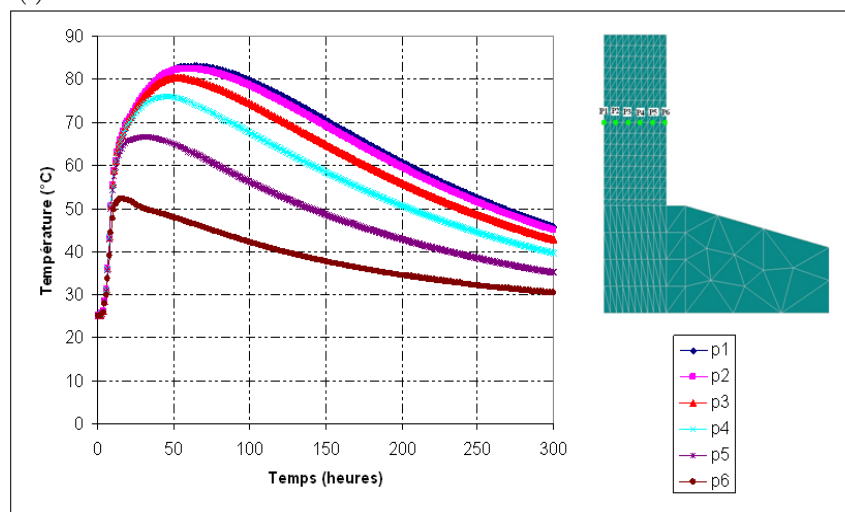


FIGURE 6: Evolution of temperature during construction at different points p1 to p6 of the pier P1 as a function of time in hours.

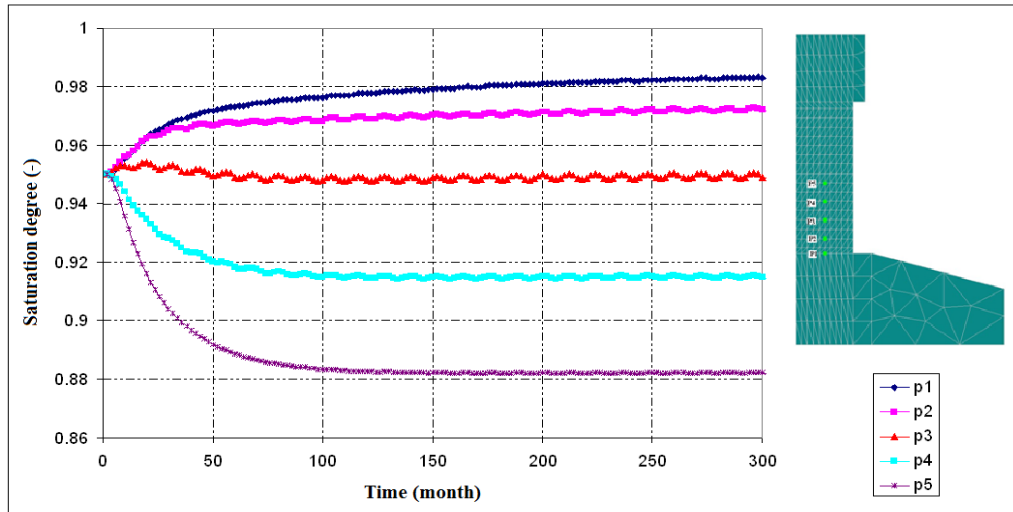


FIGURE 7: Evolution of the saturation degree at different levels p1 to p5 located in the tidal zone.

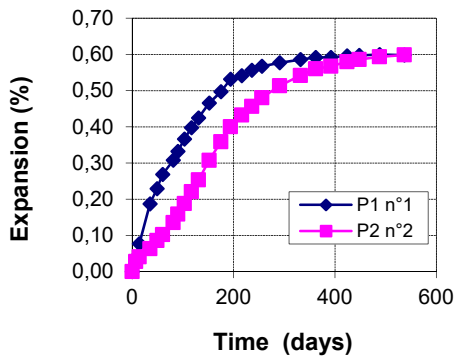


FIGURE 8: Expansion of two cores taken in the center of the piers P1 and P2.

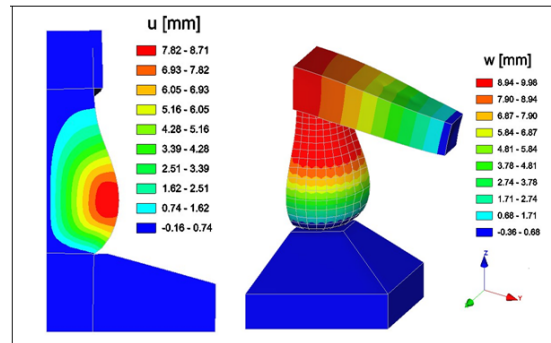


FIGURE 9: Iso-values of vertical (w) and radial (u) displacements of pier P1.

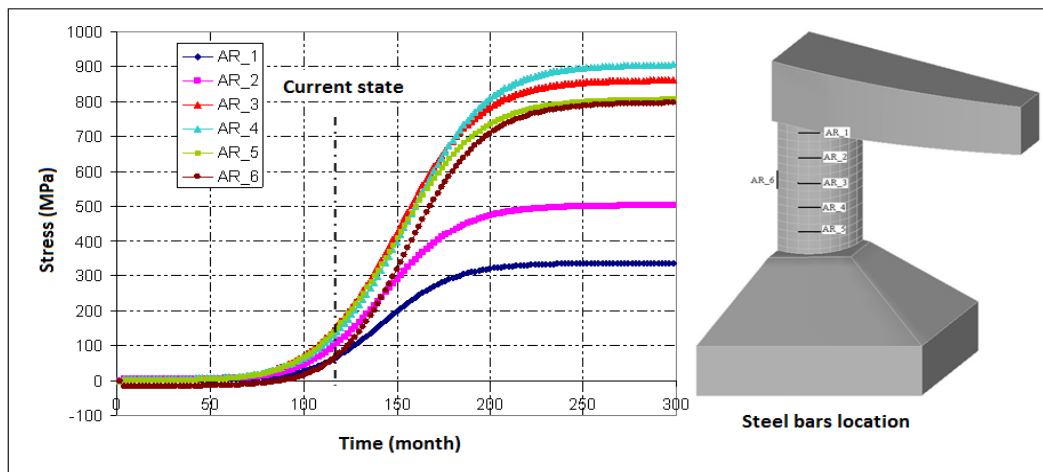


FIGURE 10: Evolution of the calculated stresses in the reinforced steel bars of pier P1.

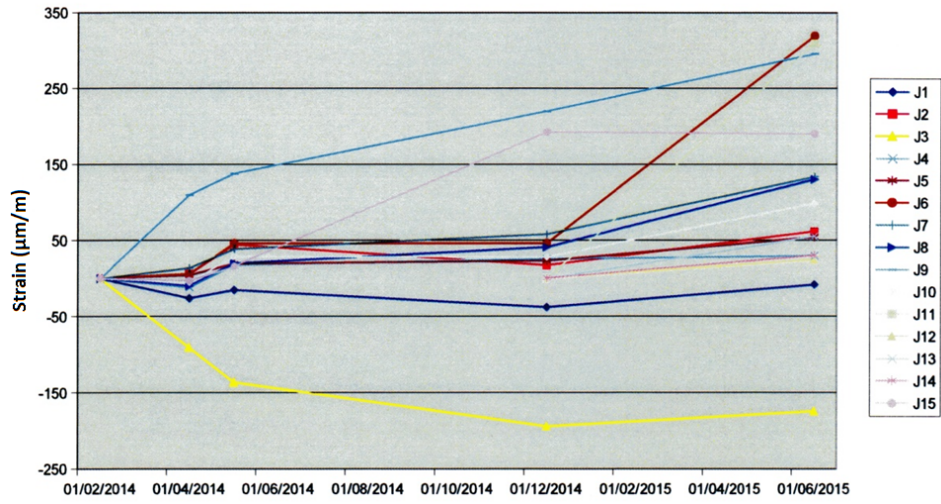


FIGURE 11: Evolution of the strains measured by the gauges from Feb 2014 to June 2015 (Pier P1).

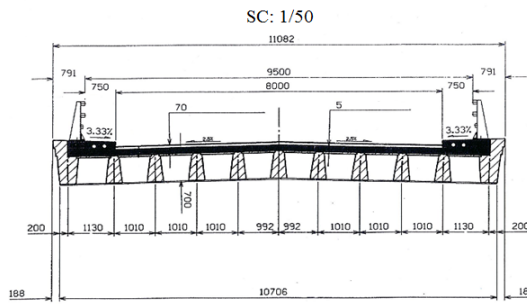


FIGURE 12: Cross-section of the bridge.

FIGURE 13: View of the cracking of an edge beam.

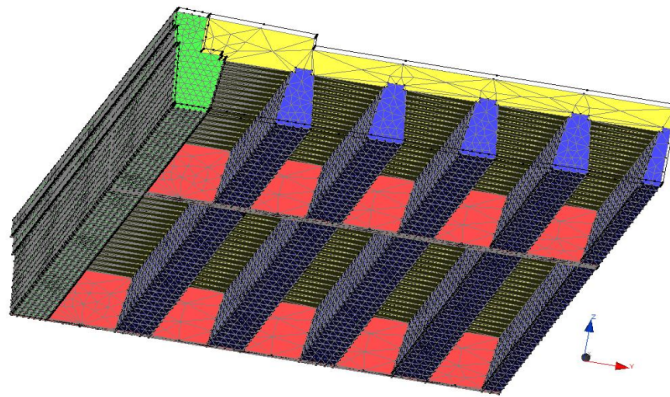


FIGURE 14: Finite element mesh used for the simulations of the bridge (view from beneath).

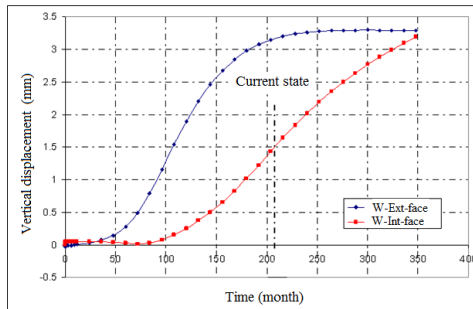


FIGURE 15: Vertical displacements between the inner and outer faces of an edge beam.

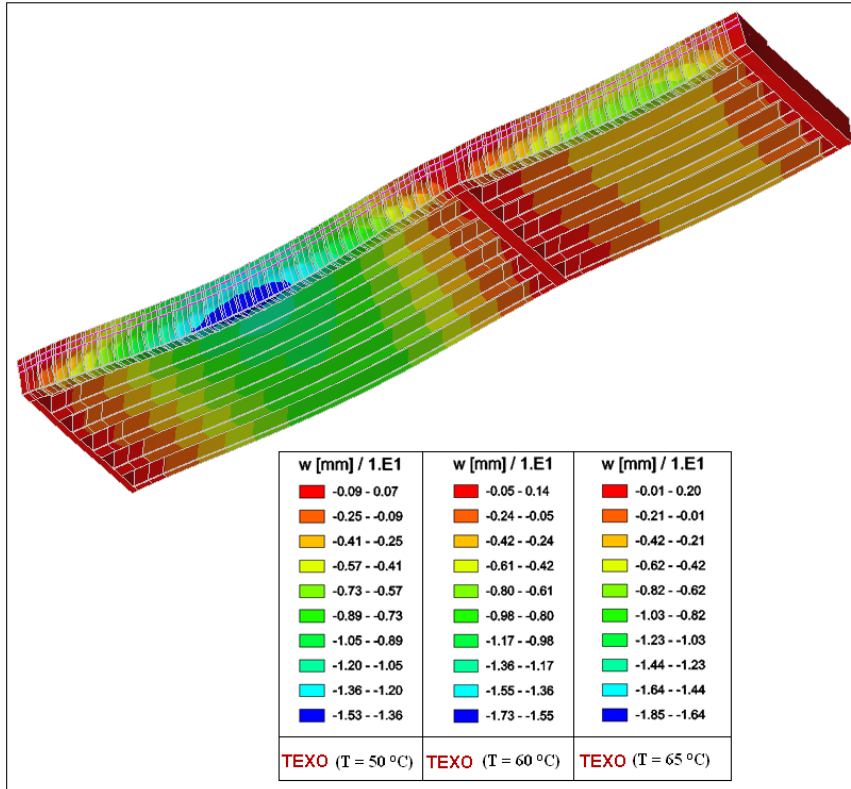


FIGURE 16: Iso-values of vertical displacements for different heat treatments cases.

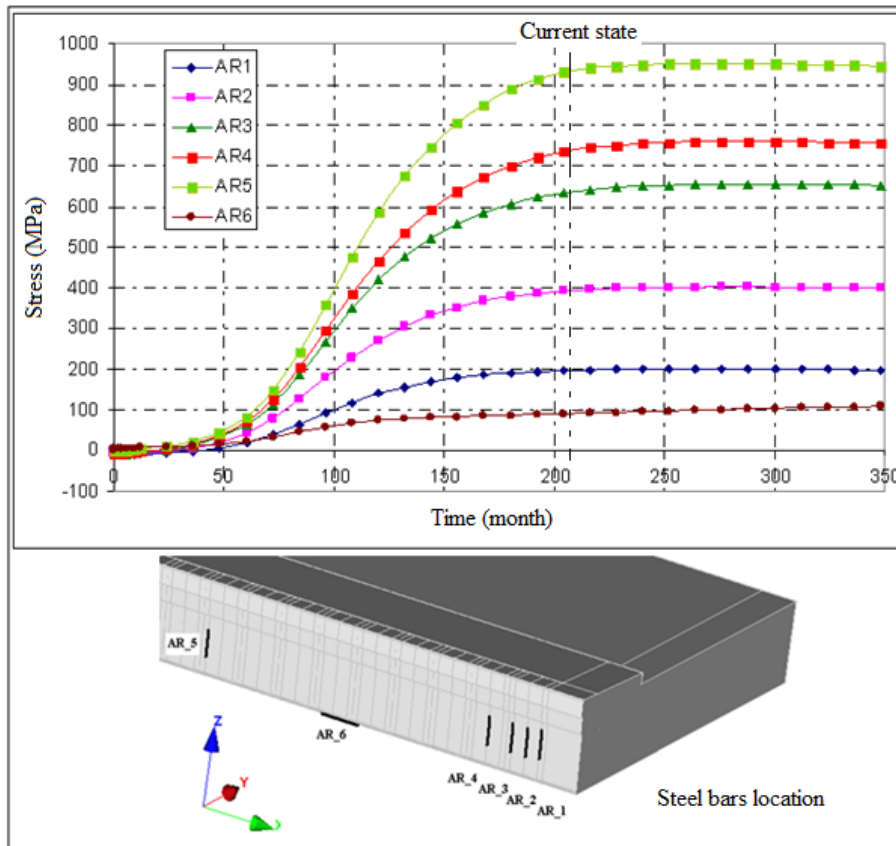


FIGURE 17: Evolution of stresses in the reinforcing steel bars of the edge beam.